General Disclaimer

One or more of the Following Statements may affect this Document

- This document has been reproduced from the best copy furnished by the organizational source. It is being released in the interest of making available as much information as possible.

- This document may contain data, which exceeds the sheet parameters. It was furnished in this condition by the organizational source and is the best copy available.

- This document may contain tone-on-tone or color graphs, charts and/or pictures, which have been reproduced in black and white.

- This document is paginated as submitted by the original source.

- Portions of this document are not fully legible due to the historical nature of some of the material. However, it is the best reproduction available from the original submission.

Produced by the NASA Center for Aerospace Information (CASI)

X-692-70-268

PREPRINT

NASA TM X-63989

MAGNETIC AND KINETIC PRESSURES IN THE SOLAR WIND

L. F. BURLAGA

K. W. OGILVIE

RECEIVED NASA STI FACILITY INPUT BRANCH AUG 1970

JULY 1970

GSFC

GODDARD SPACE FLIGHT CENTER

GREENBELT, MARYLAND

FACILITY FORM 602

N70-34445 (ACCESSION NUMBER)

(THRU)

27 (PAGES)

1 (CODE)

TMX-63989 (NASA CR OR TMX OR AD NUMBER)

29 (CATEGORY)

X-692-70-268

MAGNETIC AND KINETIC PRESSURES IN THE SOLAR WIND

L. F. Burlaga
K. W. Ogilvie

Laboratory for Extraterrestrial Physics
NASA-Goddard Space Flight Center
Greenbelt, Maryland

July 1970

Abstract

Explorer 34 solar wind data for the period June to December, 1967 show that a) The magnetic pressure, $P_B \equiv B^2/8\pi$, and kinetic pressure, $P_k \equiv n_p kT_p + n_\alpha kT_\alpha + n_e kT_e$, are variable and positively correlated on a scale of $\gtrsim 2$ days, but b) changes in P_B and P_k are anticorrelated on a scale ~1 hr (~.01 AU). Thus, dynamical hydromagnetic processes ($d\vec{v}/dt \neq 0$) must occur on the mesoscale, but the solar wind tends to be in equilibrium ($P_B + P_k \sim$constant) on a smaller scale, the microscale. The 3-hour averages show that the most probable value of $\beta \equiv P_k/P_B$ is $\beta_p = 1.0 \pm .1$, which implies that the most probable state of the solar wind at 1 AU is not one of equipartition between the kinetic energy and magnetic energy. The average total pressure for a given bulk speed ($\overline{P}(V) = P_k + P_B$) is essentially independent of V, implying that P is not determined by the heating or acceleration mechanisms of the solar wind; the average pressure is $\overline{P} = (2.9 \pm 1.5) \times 10^{-10}$ dynes/cm^2.

I. Introduction

The dynamical equation shows that motions in the solar wind are related to gradients in the pressure. Although little can be said about internal flow patterns on the basis of the existing velocity observations, it is possible to study the behavior of the solar wind pressure at 1 AU and thereby gain some insight into the dynamical state of the solar wind at 1 AU.

Previous work has indicated the usefulness of the ideas of microscale ($\sim$ 1 hr) and mesoscale ($\sim$ 2 days) in the study of the interplanetary medium (Burlaga 1969). This paper studies the dynamical state of the solar wind at 1 AU, showing that it tends to be in equilibrium on the microscale, and that dynamical hydromagnetic processes take place on the mesoscale.

The definition of the pressure and its relation to perpendicular motions are given in Section II. The observations of relations between the magnetic and kinetic pressures and the variations in the total pressure are given in Sections III and IV, and the implications of the results are discussed in the last section.

These results are based on magnetic field and plasma data from Explorer 34 for the period June to December, 1967. The plasma probe of Ogilvie and Wilkerson and the data reduction procedures are described in Ogilvie et al., (1968) and Burlaga and Ogilvie (1968) respectively. The magnetometer of Ness and Fairfield is discussed in a report by Fairfield (1969).

II. Definition of Pressures

Although there is some disagreement as to the correct equations for fluid motions in the solar wind, particularly for motions along the magnetic field direction, $\underset{\sim}{B}$, the guiding center theory, the collisionless Boltzman equation, CGL theory, and hydromagnetic theory all give the following equation for motions perpendicular to $\underset{\sim}{B}$:

$$\hat{e} \times \left(\rho \frac{d\underset{\sim}{v}}{dt} + \nabla \cdot \underset{\approx}{P}^{k} + \frac{1}{4\pi} \underset{\sim}{B} \times \nabla \times \underset{\sim}{B} \right) = 0 \qquad (1)$$

(see Whang (1970), Chandrasekhar (1960), and Burgers (1959)); here $\underset{\approx}{P}^{k} \equiv P_k^{\perp} I + (P_k^{\parallel} - P_k^{\perp}) \hat{e}\hat{e}$, where $P_k^{\perp}$ is the kinetic pressure perpendicular to $\underset{\sim}{B}$, $P_k^{\parallel}$ is the kinetic pressure parallel to $\underset{\sim}{B}$, $\hat{e}$ is a unit vector along $\underset{\sim}{B}$, and $\underset{\approx}{I}$ is a unit dyadic. The proton anisotropy is relatively large, $P_p^{\parallel} / P_p^{\perp} \approx 1.5$, but the electron anisotropy is small, $P_e^{\parallel} / P_e^{\perp} \lesssim 1.1$ and the most probable electron pressure is appreciably larger than that for the protons (Hundhausen, 1968). Thus the total kinetic pressure anisotropy (protons plus electrons) is relatively small, $(P_k^{\parallel} - P_k^{\perp}) / P_k^{\parallel} \lesssim .15$, so the anisotropy can be neglected to zeroth order. Then (1) can be written to good approximation as

$$\rho \frac{d\underset{\sim}{v}_{\perp}}{dt} = \rho \frac{\partial \underset{\sim}{v}_{\perp}}{\partial t} + \rho(\underset{\sim}{v} \cdot \nabla) \underset{\sim}{v}_{\perp} = -\nabla P - \frac{\hat{e}}{4\pi} \times (\underset{\sim}{B} \cdot \nabla) \underset{\sim}{B} \qquad (2)$$

where P is a scaler pressure given by

$$P \equiv P_k + P_B, \qquad (3)$$

$$P_B \equiv B^2/8\pi \qquad (4)$$

$$P_k \equiv \Sigma\, n_i \kappa T_i \quad \text{(sum over particle species)} \qquad (5)$$

The quantities P, P_B and P_k are the subject of this paper. Their relation to internal motions in the solar wind is given by (2).

The principal contributers to P_k are the protons , electrons and α particles. The current measurements of the electron temperature, (see Montgomery et al.,(1968) and the summary of observations in Burlaga and Ogilvie (1970)), indicate that $T_e \sim (1.4 \pm .5) \times 10^5 {}^oK$, independent of time. This is true even in the hot spots ahead of high speed streams (Burlaga et al., 1970). The α particles make only a small contribution to P_k, so to good approximation we can set n_α/n_p and T_α/T_p equal to their mean values, .045 and 3.5, respectively (see Neugebauer and Snyder, 1966 , Hundhausen et al., 1967, Robbins et al., 1970, Ogilvie and Wilkerson, 1969). The electron density is determined by the requirement of charge neutrality. These conditions give the following expression for the kinetic pressure:

$$P_k = nk\,(1.16T + 1.55\times10^5) \qquad (6)$$

where n and T are the proton density and temperature, respectively. Note that <u>electrons can play an important role in the dynamics even though their inertia is small and their temperature is nearly constant</u>.

III. Large-Scale Variations of P_k and P_B.

Positive Correlation between P_k and P_B. Figure 1 shows a macroscale view of $P_k(t)$ and $P_B(t)$ based on 3 hour averages of Explorer 34 plasma and magnetic field measurements for the period June to December, 1967. It can be seen that P_k and P_B are generally positively correlated on a scale of $\gtrsim 2$ days and that they tend to be equal. The most prominent peaks in P_k and P_B, indicated by the dashed lines in Figure 1, occur in regions where the bulk speed, V, is increasing with time. (A plot of V(t) may be found in Burlaga and Ogilvie, 1970). Thus, the highest kinetic and magnetic pressures are found at the leading edge of high speed streams. This is not surprising, since several observers have reported exceptionally high densities, temperatures and magnetic field intensities ahead of fast streams. We shall denote the 36 hour periods centered about the dashed lines in Figure 1 as "interaction regions".

The positive correlations are most marked in the interaction regions, but they are generally seen elsewhere as well. On June 21 and 22, July 7, September 6 and 11, October 3, November 6, and November 20 the correlation is negative, but most of these anticorrelations occur on a scale < 2 days.

β. The relative importance of the magnetic pressure and the kinetic pressure is given by the distribution of β,

$$\beta \equiv P_k/P_B .$$

This distribution, computed from the 3-hour Explorer 34 averages for the period in Figure 1, is shown in Figure 2. The heavy lines are for all of the data while the lighter lines are for the same data with the interaction regions removed. The two β distributions are essentially

identical. For both cases, the most probable value of β is $\beta_p = 1.0 \pm .1$, and the full width at half maximum is $\sim \pm .5$. Thus, the most probable state is one in which the total plasma kinetic pressure is equal to the magnetic field pressure. This result implies that there is not equipartition between the total thermal energy density (E) and the magnetic field energy density (P_B), since $E = 3/2\ P_k$ This is true in the interaction regions as well as outside them.

P . Having considered $P_B(t)$, $P_k(t)$ and the ratio P_k/P_B, we now examine the characteristics of the total pressure $P \equiv P_k + P_B$ which is the basic quantity in (2).

In view of the positive correlation between P_k and P_B on a scale $\gtrsim 2$ days, it is clear from Figure 1 that P is variable on a scale of $\gtrsim 2$ days. Although we observe P as a function of time, the solar wind is being convected past the spacecraft so the variation is probably due at least in part to spatial gradients in P . The gradients are much larger in the interaction regions than outside.

The distribution of the 3-hour averages of P is shown in Figure 3. The light lines are for all of the data, and the heavy lines are for the data set with interaction regions removed. To zeroth order, the two distributions are the same. For both, the most probable value is $P_p = (2.25 \pm .25) \times 10^{-10}$ dynes/cm^2 and the full width at half maximum is $\sim 1 \times 10^{-10}$ dynes/cm^2. The average value is $\bar{P} = (2.9 \pm 1.5) \times 10^{-10}$ dynes/cm^2. The large "tail" in the P distribution is due mainly to the interaction regions.

Consider the effects that an error or fluctuations in T_e would have on the P distribution. Montgomery et al. (1968) suggested that T_e ranges from $.9 \times 10^5$ °K to 2×10^5 °K. For the smaller value, $\bar{P} = (2.5 \pm 1.4) \times 10^{-10}$ dynes/cm^2 while the larger gives $\bar{P} = (3.2 \pm 1.7) \times 10^{-10}$ dynes/cm^2 where

$\overline{P}$ is the average value of P for the data set which excludes the interaction regions. Thus, the effects of the uncertainties and variations of T_e on $\overline{P}$ are small.

Now consider the variation of P with wind speed, shown in Table I for the data set which excludes the interaction regions. The result is that P is essentially independent of V between 300 km/sec and 750 km/sec. This result can be understood by examining n(V), T(V) and B(V), which are presented in Table I. The temperature increases with V, in agreement with the results in Burlaga and Ogilvie (1970). The density decreases with V. (If $n \propto V^{-x}$, x is definitely >1 and probably <2). The pressure, nkT, increases slowly with V. B is essentially independent of V between 350 km/sec and 650 km/sec, but is possibly somewhat larger than the mean, $\overline{B} = 5.4\gamma$, for V<350 km/sec and possibly somewhat larger than the mean for V>650 km/sec. Thus, the variation of P closely follows that of B. This is because a) $nkT < B^2/8\pi$ (see Burlaga et al. 1969), b) T_e is constant, c) nkT varies relatively little with increasing V.

In Figure 4 we show the dependence of $\bar{n}$ upon V for the complete data set, which indicates a monotonic decrease with n approximately proportional to $V^{-1.5}$. The mass flux is thus not constant. The $V^{-1.5}$ dependence is only approximate, since there is considerable scatter in the densities at a given V.

Figure 4 also shows average densities and velocities obtained from other experiments, as given by Hundhausen et al. (1970). The Explorer 34 averages

are systematically lower than the results obtained by the other experiments. Pioneer 6 and Vela 3 for the same period as Pioneer 6 found mean speeds of 430 km/sec and 410 km/sec, respectively, which are comparable to the Explorer 34 value of 438 km/sec. However, the corresponding Vela 3 and Pioneer 6 densities are 1.2 times the Explorer 34 value of 4.9 cm^{-3}. This difference is within the stated systematic error of 30% (Ogilvie et al., 1967). It is not possible to say which, if any, of the experiments gives the correct density.

The relationship between n and V for the data with the interaction regions removed is given in Figure 5 which shows how the data are consistent with a decrease in mass flux with increasing bulk speeds below the most probable speed around 400 km sec^{-1}. Instrumental effects would tend to an underestimate of n where V (and thus T) is low; the rise in flux at low bulk speeds thus appears real.

IV. Microscale Relations Between P_k and P_B.

Figure 6 shows a mesoscale plot of P_B, P_k and P based on the highest-time resolution plasma data from Explorer 34 (measurements made at 3 min. intervals) and the corresponding magnetic field measurements. The feature we wish to emphasize here is the anticorrelation beteen P_B and P_k which can be seen on a scale of an hour or two. This is most marked in the interaction region around 1200 UT on October 8, but it is also seen outside the interaction region. It has the effect of tending to make P a constant. Such anticorrelations are frequently seen in mesoscale plots, but the effect is not large enough to eliminate the peaks in P at the interaction regions.

Since it is not practical to show the anticorrelation for all of the data using plots such as Figure 6, we have examined it statistically as follows.

Let

$$S_j \equiv \frac{1}{N} \sum_{i=1}^{N} Sn(\bar{P}_B^j(i+1) - \bar{P}_B^j(i)) \times Sn(\bar{P}_k^j(i+1) - \bar{P}_k^j(i))$$

where Sn (x) is the algebraic sign of x, i is related to time, and the bars denote averages over a period t_j. We start with pressures at 3 min. intervals, derived from the individual measurements, to get S_1. Then successive pairs of pressures are averaged to get the 6-min. average pressures in S_2. Successive pairs of these averages are used to get S_3, etc. If P_B and P_k are perfectly anticorrelated on a scale t_j ($t_{j+1} = 2t_j$; t_1=3 min), then S_j = -1; if they are perfectly correlated, S_j=+1, and if they are uncorrelated, S_j=0.

Since the Explorer 34 interplanetary data are interrupted by passages into the magnetosheath, we have computed S_j, j=1 to 9, for

each ~4 day orbit, i.e., $2^{10}=1024$ points were used for each orbit. Since each point was separated by 3 min, this represents a period of somewhat more than 2 days per orbit. Orbits for which the spacecraft spent less than 2 days in the solar wind and orbits with data gaps were not used. The total number of orbits for which S_j (j=1,9) could be computed is 33. Having 33 values of each S_j, the averages of these were computed to obtain the result shown in Figure 7. On a scale of 3 min S_j is negative but $|S_j|$ is small, indicating a weak anticorrelation which is obscured by measurement uncertainties. On a scale of ~ 1 hr one sees a distinct anticorrelation between changes in P_B and P_k. This disappears on a larger scale, where correlation drops to zero, and on a scale of $\gtrsim$10 hr. there is evidence that changes in P_B and P_k are positively correlated in agreement with the conclusions in Section III. There is a large statistical error in each of the points in Figure 7 ($\sigma(S_j) \sim S_j$), and the measurement errors reduce the magnitude of the anticorrelation, but this does not change the conclusions.

V. Discussion and Summary.

The solar wind pressure for the period June to December, 1967, is described by the following macroscale statistics: a) The most probable pressure $P = P_B + P_k$ was $(2.2 \pm .3) \times 10^{-10}$ dynes/cm^2 and the average was $(2.9 \pm 1.5) \times 10^{-10}$ dynes/cm^2, b) $\overline{P}$ (V) was essentially independent of the bulk speed, c) The most probable value of $\beta = P_k/P_B$ was $\beta_P = 1.0 \pm .1$.

The observed average P is simply that which is expected from the well known average density, temperatures and magnetic field intensity. The reasons for result b) are given in Section III. It should be noted that the effect of interaction regions on the P(V) relation is small, so that the independence of $\overline{P}$ (V) and V refers to the macroscale characteristics of the solar wind. The implication of this result is that the mean pressure at a given speed is not determined by the mechanism which gives rise to that speed. Since a given speed implies a given temperature at any part of the solar cycle (Burlaga and Ogilvie, 1970), the mean $\overline{P}$(V) is also essentially independent of the heating mechanism. These results put a further constraint on the heating and acceleration mechanisms, namely that they should operate without changing the pressure.

The third result above, $\beta_P = 1.0 \pm .1$, implies that the most probable state of the solar wind is not one of equipartion between the total kinetic energy and magnetic energy. Thus, either there is a dynamical process at 1 AU which maintains $\beta_P = 1$ or the result is determined by conditions at the sun and $\beta_P = 1$ is coincidental. If the first case is correct, one expects to find $\beta_P = 1$, independent of the distance of the sun, in an extended region near the earth. A third possibility, that $\beta_P = 1$ is incorrect due to experimental uncertainties, cannot be excluded because of the difficulty in absolutely calibrating plasma

probes. Vela 3 and Pioneer 6 average densities were 1.2 times the Explorer 34 average density, for similar average speeds. Thus, it is possible that $\beta_p = 1.2$, but this still implies the absence of equipartition between the particles and field. The result $\beta=1$ (or $\beta = 1.2$) is inconsistent with that of Neugebauer and Snyder (1967), who found an equipartition between the positive-ion thermal energy density and the magnetic energy density during the period April 28 to November 18, 1962.

A positive correlation between $P_B(t)$ and $P_k(t)$ is seen on a scale $\gtrsim$ 2 days, while a negative correlation if found on a scale of 1 or 2 hours. The positive correlation is most marked by large increases in P_B and P_k at the leading edge of high speed streams, and is simply a manifestation of the well-known "piling-up" effect. But positively correlated variations in P_B and P_k also occur away from the interaction regions. Both the interaction regions and the remaining regions can be expected to give rise to internal motions at 1 AU. Since $\beta \sim 1$, we emphasize that these must be treated as hydromagnetic motions. The accelerations are likely to be greatest in the interaction regions because the pressure gradients are largest there. The anticorrelation between changes in P_k and P_B on a scale of $\sim$ 1 hr is a general feature of the solar wind which is seen both in the interaction regions and outside them. It suggests that $P = P_B + P_k \sim$ constant on the microscale. Thus regions on the microscale in which there is approximate equilibrium take a part in dynamical motions on the large scale. The difference in the correlation between P_B and P_k observed for the meso and microscales shows the validity and usefulness of these concepts in connection with the interplanetary medium.

FIGURE CAPTIONS

Figure 1 Plots of the magnetic pressure P_B and kinetic pressure P_k, showing positive correlation on a scale $\gtrsim$ 2 days. Peaks and gradients in P_B and P_k are generally greatest at the leading edge of high speed streams, indicated by the vertical dashed lines. Data are for solar rotations 1831 to 1838.

Figure 2 The normalized distribution of β computed from 3-hr averages of the plasma and magnetic field parameters for the period June-November, 1967. The most probable value is $1.0 \pm .1$. The distribution of β in the interaction regions is the same as outside these regions.

Figure 3 The normalized distribution of P computed from 3-hr averages of the plasma and magnetic field parameters for the period June-December 1967. There are relatively more high values of P in the set of data which includes the interaction regions. The average value of P is $\bar{P} = (2.9 \pm 1.5) \times 10^{-10}$ dynes/cm^2.

Figure 4 Density versus bulk speed from the Explorer 34 3-hr averages. The simple relation shown here is somewhat misleading since there is considerable scatter in the actual values. The variances in n are $\approx$50% of the average values which are plotted here.

Figure 5 Mass flux versus bulkspeed for the data with the interaction regions removed. The mass flux decreases with bulk speed when $V < 500$ km/sec.

Figure 6 Anticorrelation between changes in P_B and P_k. Several regions can be seen in which there is an anticorrelation on a scale of an hour. This tends to reduce the variations in P, but the peak at 1200 UT on October 8 shows that large increases in P occur despite the anticorrelation.

Figure 7 S_j measures the correlation between changes in P_B and P_k for various scales. A distinct anticorrelation is seen on a scale of 1 hr ~ .01 AU but they tend to be correlated on a larger scale.

REFERENCES

1. Burgers , J. M. : 1959, "Statistical Plasma Mechanics", in Symposium of Plasma Dynamics, ed. F. H. Clauser, Addison-Wesley, Reading, Mass.

2. Burlaga, L. F. : 1969, Solar Physics, 7, 54.

3. Burlaga, L. F. and Ogilvie, K.W.:, 1968, J. Geophys. Res. 73, 6167.

4. Burlaga, L. F. and Ogilvie, K. W.:, 1970, Astrophys. J. 159, 659.

5. Burlaga, L. F., Ogilvie, K.W., and Fairfield, D. H. 1969, Astrophys. Journal, 155, L171.

6. Burlaga, L. F., Ogilvie, K. W., Fairfield, D. H., Montgomery, M.D., and Bame, S. J.: 1970, submitted to Astrophys. J.

7. Chandrasekhar, S.: 1960, Plasma Physics, The University of Chicago Press, Chicago.

8. Fairfield, D. H.: 1969, J. Geophys. Res. 74, 3541.

9. Hundhausen, A. J. : 1968, Space Sci. Rev. 8, 690.

10. Hundhausen, A. J., Asbridge, J. R., Bame, S. J., Gilbert, H. E., and Strong, J. B.: 1967, J. Geophys. Res. 72, 87.

11. Hundhausen, A. J., Bame, S. J., Asbridge, J. R., and Sydoriak, S. J.: 1970, Preprint.

12. Montgomery, M. D., Bame, S. J., and Hundhausen, A. J.: 1968, J. Geophys. Res. 73, 4999.

13. Neugebauer, M. and Snyder, C. W.: 1966, J. Geophys. Res. 71, 4469.

14. Neugebauer, M. and Snyder, C. W.: 1967, J. Geophys. Res. 72, 1823.

15. Ogilvie, K. W., Burlaga, L. F., and Wilkerson, T. D.: 1968, J. Geophys. Res. 73, 6809.

16. Ogilvie, K. W., Burlaga, L. F. and Richardson, H.: 1967, NASA X-612-67-543.

17. Ogilvie, K. W. and Wilkerson, T. D.: 1969, Solar Physics, 8, 435.

18. Robbins, D. E., Hundhausen, A. J., and Bame, S. J.: 1970, J. Geophys. Res. 75, 1178.

19. Whang, Y. C.: 1970, NASA/GSFC Preprint X-692-70-61.

ACKNOWLEDGEMENTS

We wish to thank Dr. N. Ness and Dr. D. Fairfield for providing their magnetic field data for this study. Mr. T. Carlton and Mr. M. Courtney did the programming. Dr. Fairfield has critically examined the manuscript and offered helpful comments.

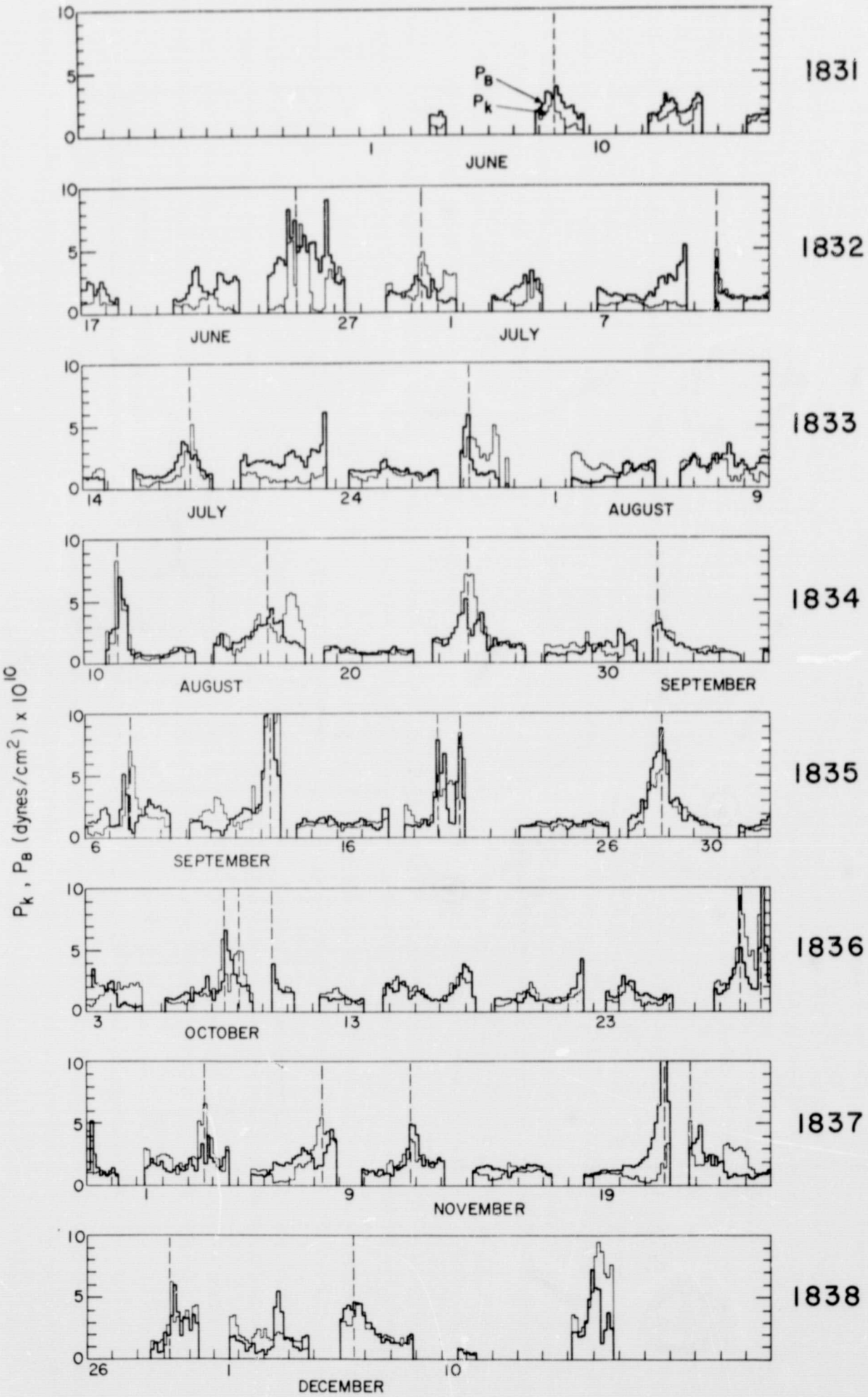
P_k , P_B (dynes/cm^2) x 10^{10}
P_B
P_k
1831
1
10
JUNE
1832
17
JUNE
27
1
JULY
7
1833
14
JULY
24
1
AUGUST
9
1834
10
AUGUST
20
30
SEPTEMBER
1835
6
SEPTEMBER
16
26
30
1836
3
OCTOBER
13
23
1837
1
9
NOVEMBER
19
1838
26
1
DECEMBER
10

Figure 1

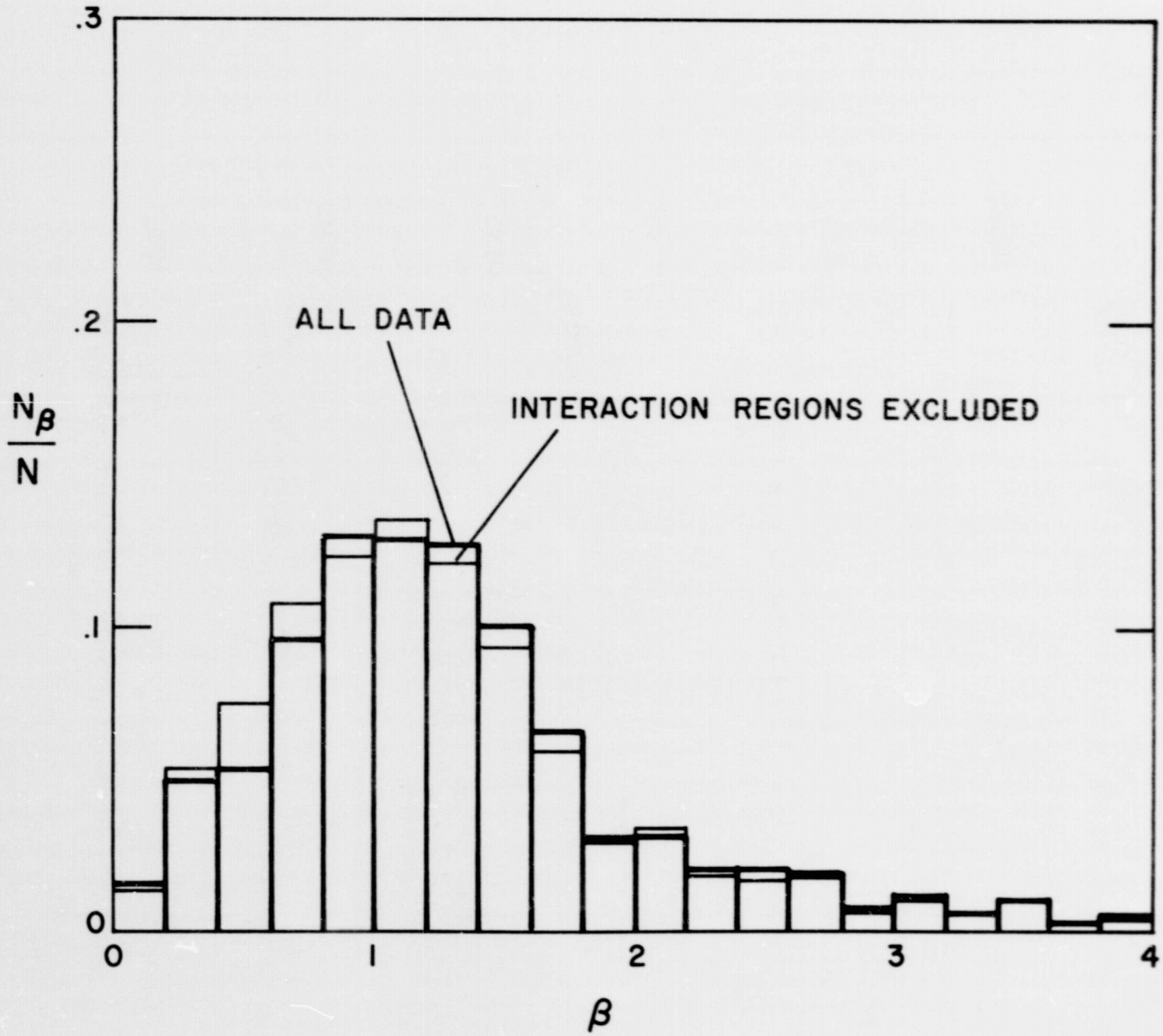
.3
.2
.1
0
$\frac{N_\beta}{N}$
ALL DATA
INTERACTION REGIONS EXCLUDED
0
1
2
3
4
β

Figure 2

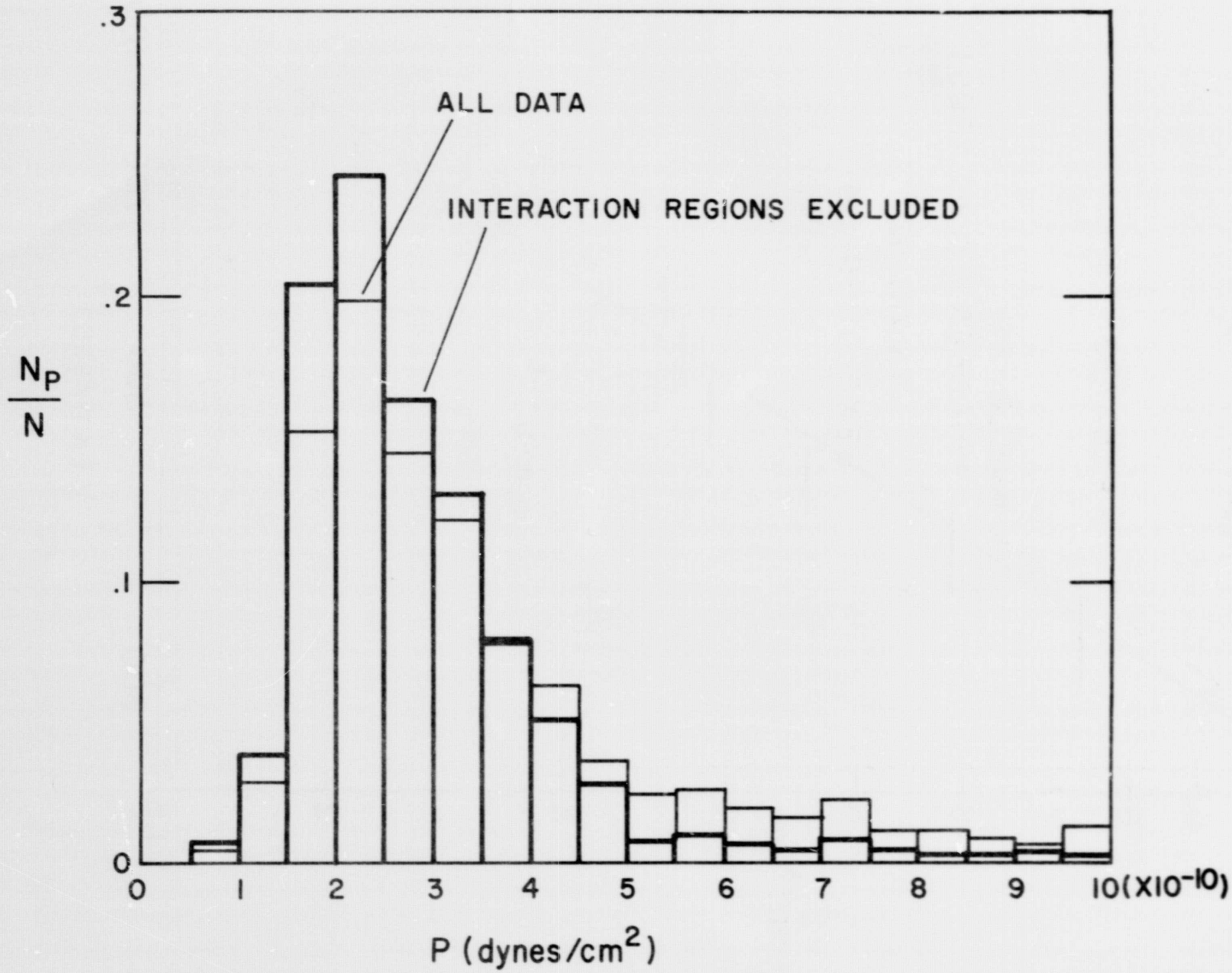
.3
.2
.1
0
ALL DATA
INTERACTION REGIONS EXCLUDED
$\frac{N_P}{N}$
0
1
2
3
4
5
6
7
8
9
10(X10^{-10})
P (dynes/cm^2)

Figure 3

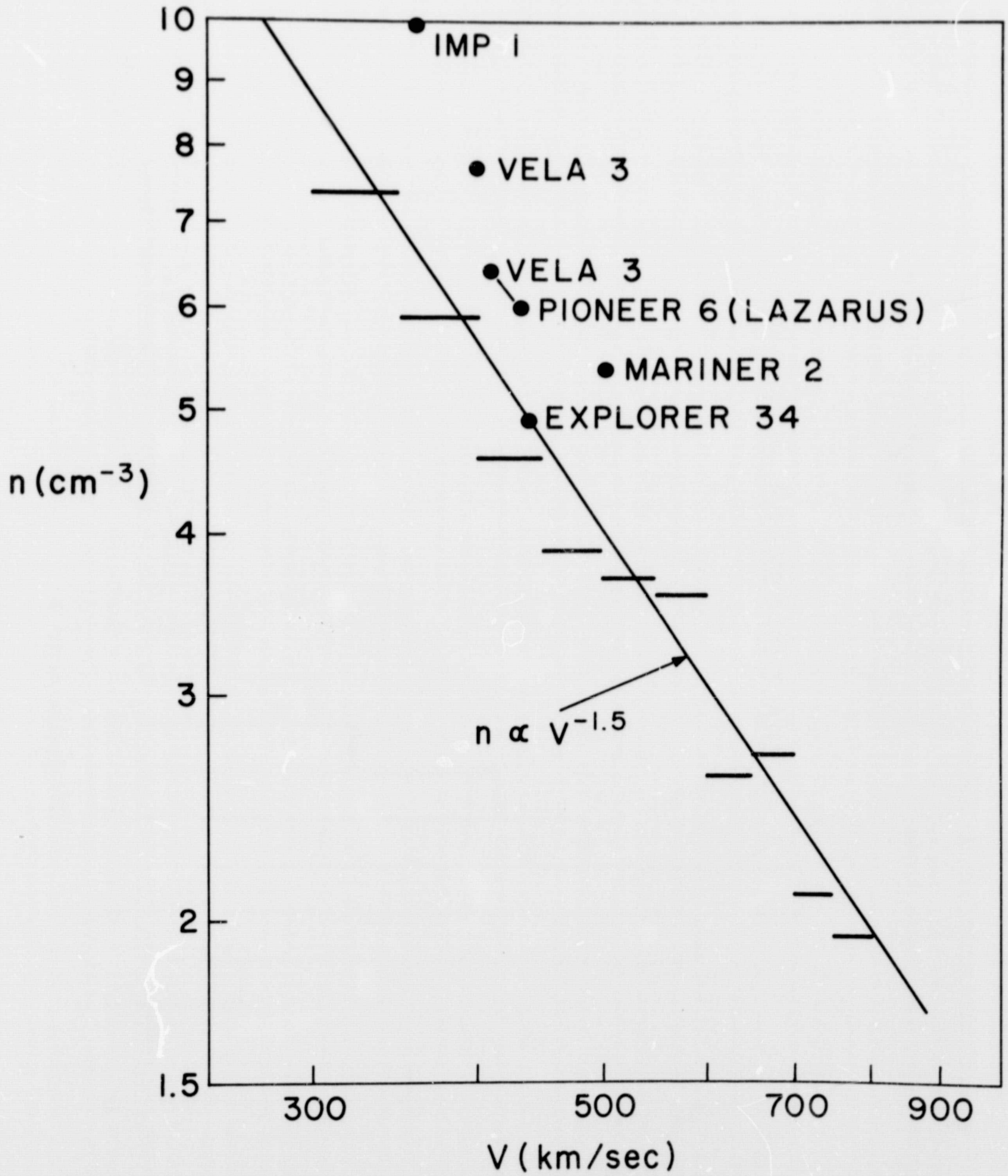
IMP I
VELA 3
VELA 3
PIONEER 6 (LAZARUS)
MARINER 2
EXPLORER 34
n (cm⁻³)
n ∝ V^-1.5
10
9
8
7
6
5
4
3
2
1.5
300
500
700
900
V (km/sec)

Figure 4

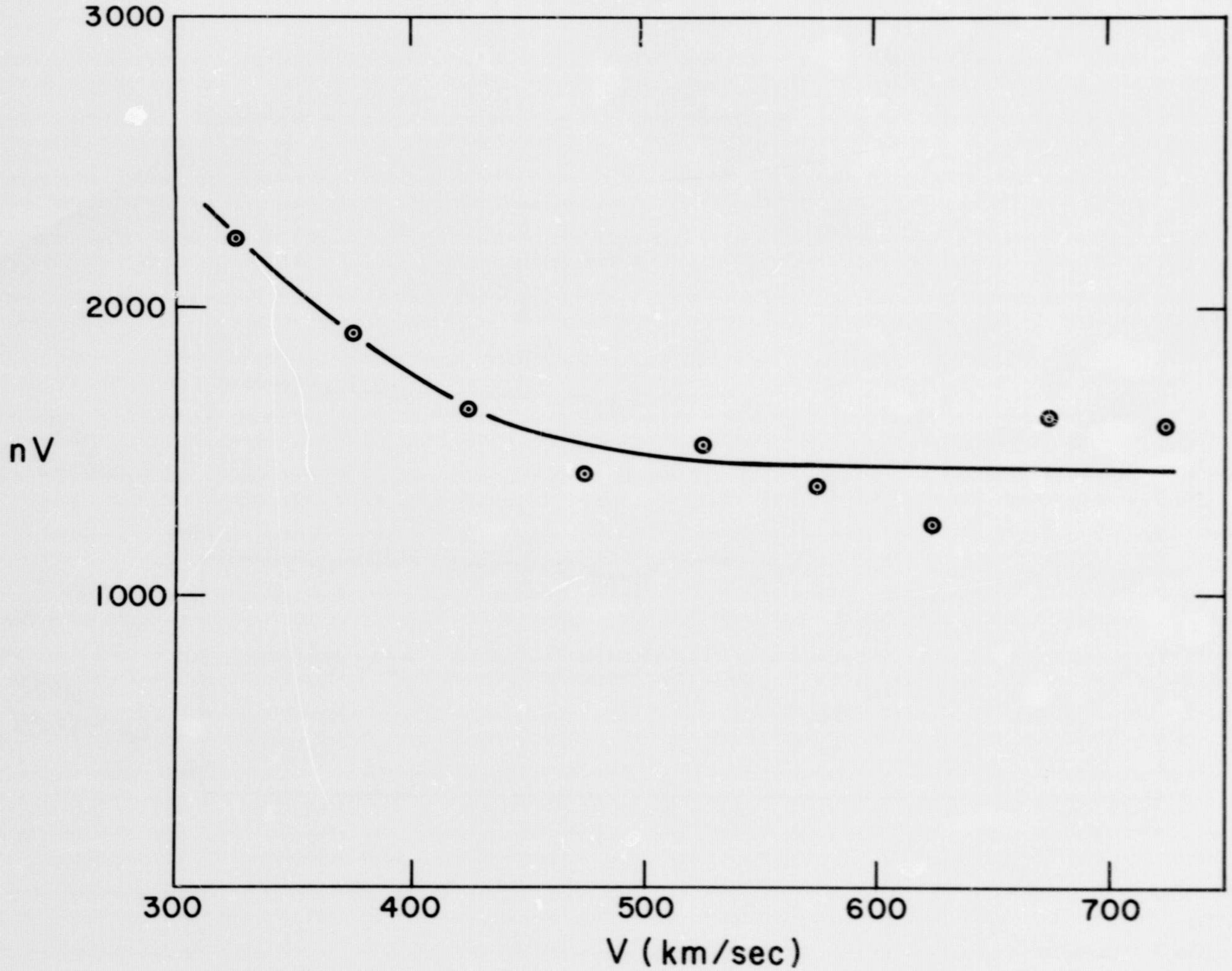

Figure 5

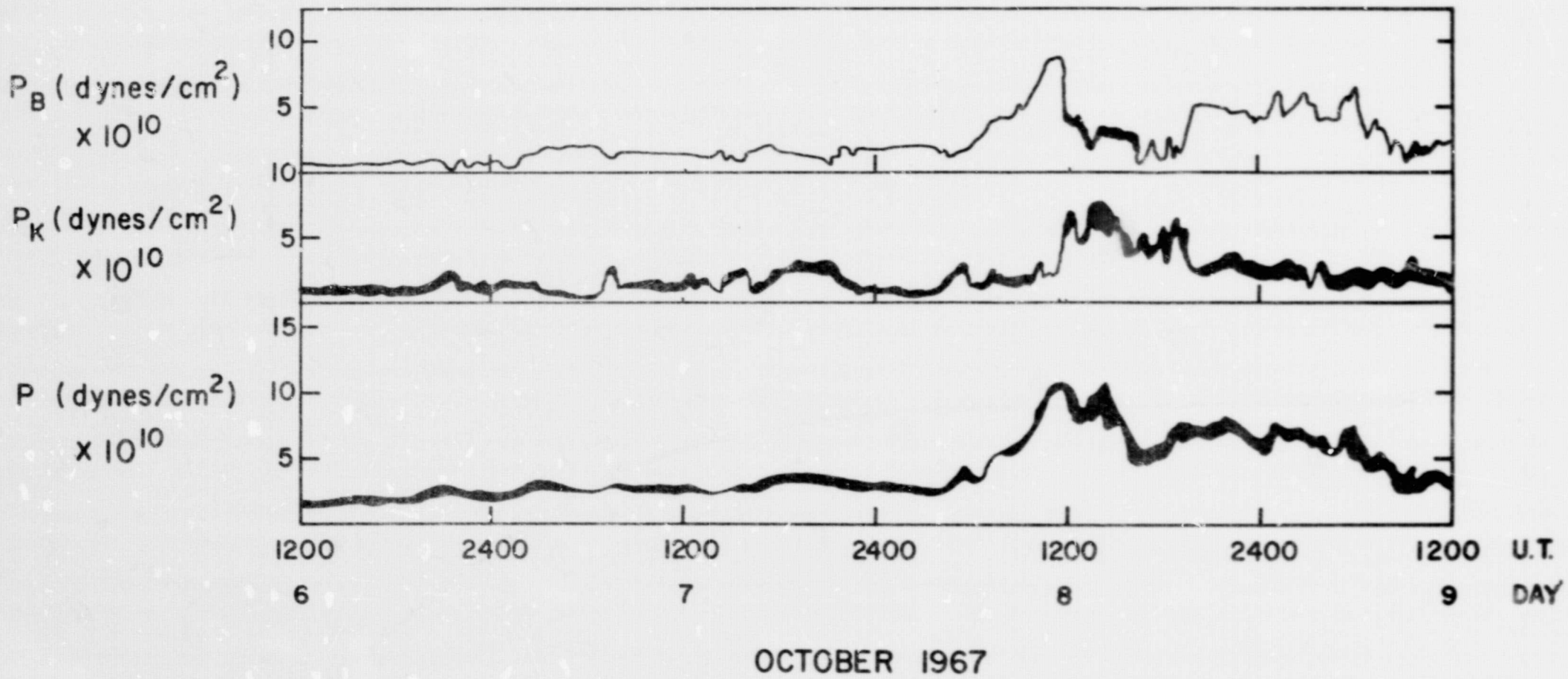
P_B (dynes/cm^2) x 10^{10}
P_K (dynes/cm^2) x 10^{10}
P (dynes/cm^2) x 10^{10}
10
5
10
5
15
10
5
1200
2400
1200
2400
1200
2400
1200
U.T.
6
7
8
9
DAY
OCTOBER 1967

Figure 6

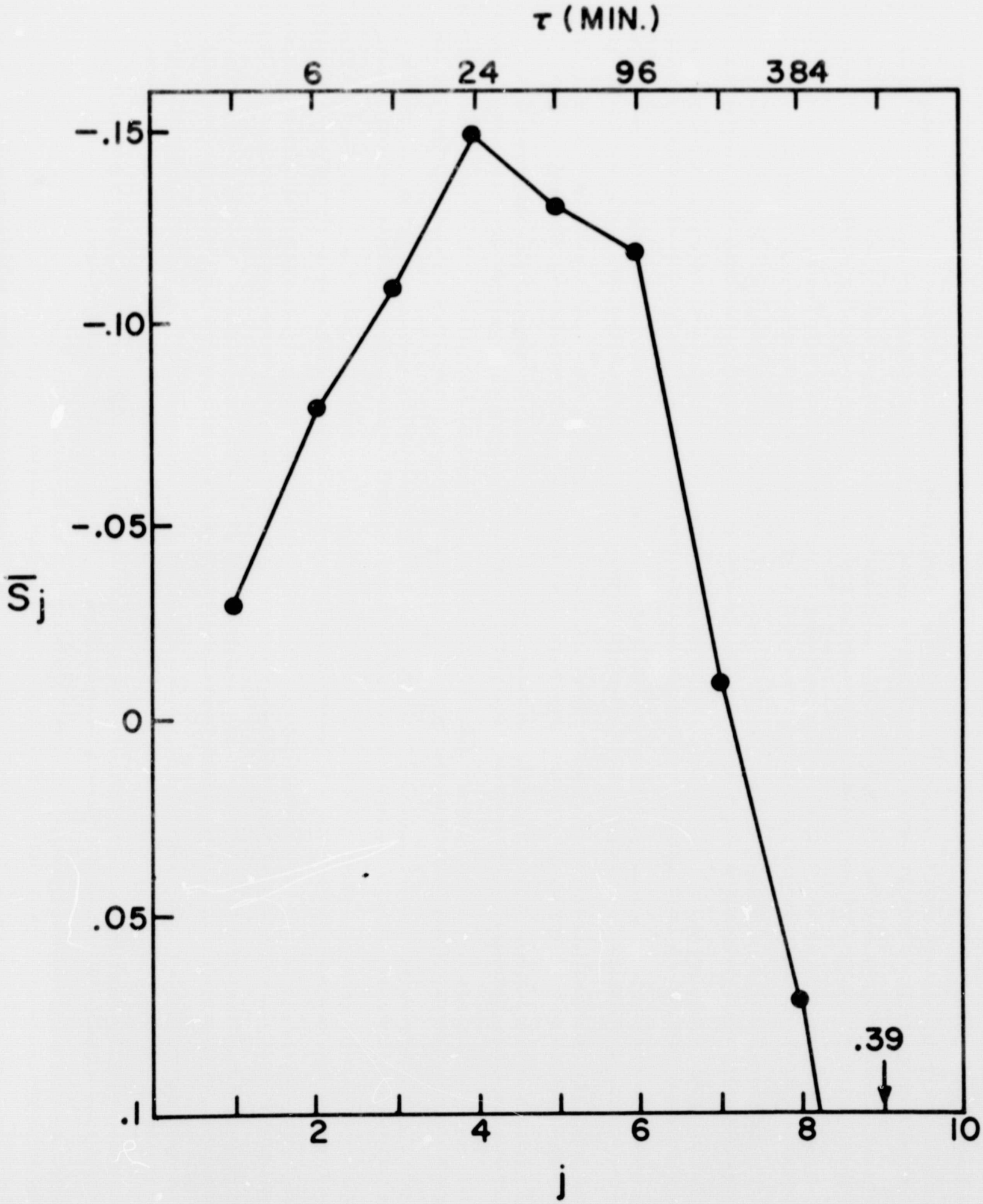

Figure 7

TABLE I

V(km/sec)	n(cm^{-3})	T_p(kilo ^oK)	B(γ)	P x10^{10} dynes/cm^2	N
300-350	7.0±3.7	40±17	4.6±1.4	2.9±1.0	128
350-400	5.1±2.7	55±26	5.6±1.9	3.0±1.6	214
400-450	3.9±2.9	99±44	5.7±1.8	2.9±1.8	197
450-500	3.0±1.2	118±59	5.7±1.7	2.8±1.5	105
500-550	2.9±1.2	127±53	5.3±1.5	2.6±1.4	64
550-600	2.4±1.2	148±64	5.6±1.6	2.8±1.8	45
600-650	2.0±.8	161±58	5.4±1.0	2.4±.9	16
650-700	2.4±.9	194±60	6.7±1.7	3.9±1.9	7
700-750	2.2±.6	185±38	6.5±.7	3.5±.8	9